Universidad de los Andes

Faculty of Science

Physics Department

Phenomenological Study of Heavy Neutrinos at the LHC Using the Vector Boson Fusion Technique

Author:

Carlos Miguel Patiño

Advisor: Carlos Andrés Flórez

Bogotá D.C. 2017

Contents

List of Figures

Chapter 1

Introduction

The standard model (SM) gathers the entire understanding about fundamental particles and their interactions. Although the model has successfully explained various physical phenomena observed experimentally, there are still multiple unanswered questions concerning particle physics. For example, experiments [1] have shown that accelerator and reactor, solar, and atmospheric neutrinos have mass by proving the existence of neutrino oscillations. The fact that there are neutrino oscillations contradicts the SM, because this model predicts that neutrinos are massless. Some specific experiments for each neutrino category are: Super-Kamiokande [2] for solar and atmospheric neutrino oscillations, KamLAND [3] for reactor neutrinos, and K2K [4] for accelerator neutrino oscillations [5]. An additional open question about neutrinos is the fact that only neutrinos with left helicity have been observed. Helicity is defined as the projection of the particle's momentum vector over its spin direction. Therefore, only neutrinos with spin anti-parallel to its linear momentum have been detected.

In order to provide neutrinos with mass, several theories that extend the predictions of the SM have been proposed. One of the most known models is the "see-saw" or balance mechanism [6]. This mechanism postulates the existence of a yet undetected particle called the heavy neutrino. This heavy neutrino would have a mass inversely proportional to the one of the neutrino, thus making the mass of the heavy neutrino considerably large. Also, this neutrino would have a right he-

licity therefore restoring the right-left symmetry in the standard model. Other models that try to provide mass to the neutrinos by extending the SM postulate the conservation of the $(B - L)$ number, where B is the baryon number and L is the lepton number. Unlike these models, the see-saw mechanism proposes a breaking in the $(B - L)$ symmetry with consequences discussed in the next paragraph.

The see-saw mechanism includes three sub-models that provide mass to neutrinos. These three models come from the fact that is necessary to take into account the effects of breaking the $(B - L)$ symmetry. This effects can be parametrized using a Weinberg operator of the form $\lambda_{ll'} L_l L_{l'} \Phi\Phi/\Lambda$ where $\Phi = (\phi^+, \phi^0)^\intercal$ is the doublet associated with the SM Higgs Boson and $L_l = (\nu_l, l)^\intercal_L$ the representation of a doublet field associated with the lepton number +1 [6]. Since there are only three ways in which this Weinberg operator can be obtained at tree-level, there are also three types of the see-saw mechanism. In the type I see-saw mechanism the product between L_l and Φ results in a fermionic singlet state . In the type II see-saw mechanism, the product between L_l and $L_{l'}$ forms a scalar triplet. Finally, the product between L_l and Φ in the type III sub-model results in a fermionic triplet state. The state formed by the products described in each see-saw model would correspond to the definition of heavy neutrino in each sub-model. Taking into account the elements described above regarding the see-saw mechanism, if heavy neutrinos are observed, the left and right symmetry in the SM would be restored and the mechanism by which the neutrinos acquire mass would be explained.

Heavy neutrinos searches have been conducted in multiples experiments, but none has been able to prove that heavy neutrinos exist. Examples of these experiments can be found in collaborations such as LEP [7], CMS and ATLAS [8]. In order to understand heavy neutrino searches it is necessary to define the concept of jet. A jet at phenomenological level is defined as a quark or a gluon. In high energies experimental physics, a jet is defined as a collection of particles resulting from the fragmentation of quarks or gluons. Searches at CMS and ATLAS have focused in final states with associated leptons and jets. Figure 1.1 shows a Feynman diagram of the production of a heavy neutrino mediated by a W boson with left or right helicity. The final state for this

process has two leptons (μ, e, or τ) and two jets.

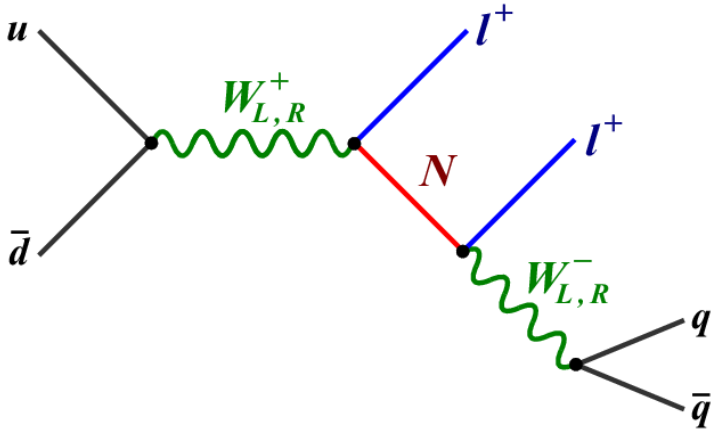

Figure 1.1: Feynman diagram of heavy neutrino production. (Taken from [8])

The main objective of this monograph is to perform a phenomenological study about the feasibility of conducting an experimental analysis for the detection of heavy neutrinos in the Large Hadron Collider (LHC) using a technique known as vector boson fusion (VBF). This technique has been recently used in the LHC [9] in searches for new physics. In high energy physics, the bosons $W^{\pm}$, Z^0 and γ are known as vector bosons. The process of vector boson fusion occurs through an electroweak interaction of associated quarks with the LHC proton beams. The VBF topology consists in requiring two highly energetic jets in the longitundinal region of the detector and in opposite hemispheres thereof. It has been shown that by requiring this type of event, the noise level (background) is reduced considerably in regions of difficult study in searches of new physics.

In order to conduct the analysis, it is important to simulate signal

and background processes and to perform a detailed physical study of the variables that allow to distinguish signal for experimental noise. It is necessary to use a cuantitative estimator commonly known as figure of merit to determine optimal cuts in the mentioned variables. The latter with the objective of reducing the amount of experimental noise by finding the optimal cuts in the relevant variables. For this particular analysis, the significance formula that will be used is the one shown in Equation 1.1, where S is the significance, $N(s)$ is the number of signal events, and $N(B)$ is the number of background events.

$$S = \frac{N(s)}{\sqrt{N(s) + N(B)}} \tag{1.1}$$

Furthermore, it is important to establish the expected experimental sensitivity using maximum likelihood limits or the calculation of the final significance for different hypothetical signal points. The procedure described would allow to conclude whether a study for the detection of heavy neutrinos at the LHC is feasible or not.

Chapter 2

Objectives

2.1 General Objectives

Conduct a phenomenological study to determine the possible experimental sensitivity of heavy neutrino searches in the LHC, using the VBF topology, in channels with high-mass resonance production.

2.2 Specific Objectives

- Develop the signal events and experimental noise simulations using MadGraph, Pythia, and Delphes software.
- Write an analysis code using ROOT software to analyze the simulated data.
- Conduct a physical study of the appropiate cinematic and topological variables that show strong separation between signal and background.
- Find the optimal cut points of the relevant physical variables using a significance figure.
- Conduct a statical analysis of the results.

Chapter 3

The Neutrino Mass

The Standard Model predicts that the neutrino is a massless particle. However, experiments like the ones mentioned in Chapter 1 have proven that neutrino oscillations exist. These oscillations show that, contrary to the predictions of the Standard Model, neutrinos are particles with mass. In this chapter, the mechanisms by which neutrinos can acquire mass in the Standard Model are given followed by the reasons that do not allow to add mass to the neutrinos int the SM. Also, the See Saw mechanism is described in greater detail.

3.1 The Dirac Mass

A standar Dirac free fermion can be described using the Langrangian shown is Equation 3.1 [14], where $\not{\partial} = \gamma^\mu \partial_\mu$ and m is the mass of the particle. Since the mass term in this Langragian is $-m\bar{\psi}\psi$, a mass term of this form is always called a Dirac mass term. The best known description for a neutrino is the a neutral standard Dirac particle. That is, a neutrino can be described by the Langrangian showed in Equation 3.1, where ψ would be four component Dirac field ν describing the neutrino.

$$\mathcal{L} = \overline{\psi}\left(i\not{\partial} - m\right)\psi \tag{3.1}$$

If the field ψ is decomposed into the corresponding left and right chiral states, the Dirac mass term can be written as

$$m(\overline{\psi_L + \psi_R})(\psi_L + \psi_R)$$

As shown in Appendix A, the terms $\bar{\psi}_R\psi_R$ and $\overline{\psi}_L\psi_L$ are zero. Therefore, the Dirac mass term can be written as shown in Equation 3.2.

$$m\left(\overline{\psi}_L\psi_R + \overline{\psi}_R\psi_L\right) \tag{3.2}$$

3.2 The Majorana Mass

The Majorana neutrino (ν_M) is a neutrino proposed by Majorana in 1937 that satisfies the property shown in Equation 3.3, where $\mathbf{C}$ is the charge conjugation operator [14]. This charge conjugation operator transforms a free neutrino state into an anti-neutrino state. Taking the latter into account, Equation 3.3 implies that the Majorana neutrino is its own anti-particle.

$$\nu_M = \nu_M^C \equiv \mathbf{C}\nu_M\mathbf{C^{-1}} \tag{3.3}$$

As in the case of a Dirac fermion, a Lagrangian like the shown in Equation 3.4 can be defined. The factor 1/2 is added to take into account double counting when an interaction term is added to the Lagrangian.

$$\mathcal{L} = \frac{1}{2}\overline{\nu}_M\left(i\partial\!\!\!/ - m\right)\nu_M \tag{3.4}$$

Once a neutrino that is its own anti-particle is defined, additional terms of the form $\overline{\nu^C}\nu^C$, $\overline{\nu^C}\nu$, and $\overline{\nu}\nu^C$ can be added to the mass term shown in Equation 3.2 [14]. The addition of these terms does not violate charge conservation, because neutrinos are neutral particles. Hence, the Lorentz invariance in the Lagrangian is being conserved. The term $\overline{\nu^C}\nu^C$ is identical to $\overline{\nu}\nu$ except for an irrelevant surface term, so it would not be necessary to include it in the mass term in Equation 3.2 [14]. However, the other two terms mentioned above are not included in this mass term, so they should be added to the general mass lagrangian. These two new

mass terms, taking into account an hypothetical neutrino with right helicity, would be like the ones shown in Equations 3.5 and 3.6.

$$\mathcal{L} \sim m_L \left(\overline{\nu^C}_L \nu_L + \overline{\nu}_L \nu_L^C \right) \tag{3.5}$$

$$\mathcal{L} \sim m_R \left(\overline{\nu^C}_R \nu_R + \overline{\nu}_R \nu_R^C \right) \tag{3.6}$$

If a Majorana neutrino is constructed as $\nu_M \equiv \nu_L + \nu_L^C$, Equation 3.5 can be written like in Equation 3.7. A similar definition can be made with an hypothetical neutrino with right helicity, so Equation 3.6 can also be written as 3.7. As in the Dirac case, Equation 3.7 is defined as the Majorana mass term. However, contrary to the Dirac mass term, the Majorana mass term can be constructed using either only ν_L or ν_R [14].

$$\mathcal{L} \sim m \overline{\nu}_M \nu_M \tag{3.7}$$

3.3 Neutrino Mass in the Standard Model

As mentioned in Chapter 1, the Standard Model only includes a neutrino with left chirality. As shown in Equation 3.2, the abscence of a neutrino with right chirality makes that all the terms in the Dirac mass Lagrangian vanish. Therefore, it is not possible to add mass to the neutrinos in the Standard Model using a Dirac mass term.

Another mechanism that could provide mass to the neutrino in the Standard Model is the Majorana mass term. However this term would not conserve the Lepton number, i.e. would violate the L symmetry, that is conserved throughout the Standard Model[15]. This happens because the Majorana fermions, in this case neutrinos, are their own antiparticles. A lepton number of $L = +1$ is assigned to a fermion and $L = -1$ to its antiparticle. Since the Majorana neutrinos are their own antiparticles, they do not have a well defined lepton number (it could be either +1 or -1). That is why the lepton number for both Majorana neutrinos would be either $L = 1$ or $L = -1$, so the Majorana mass term would violate de lepton conservation number by $\Delta L = \pm 2$. Also, some non-pertubative effects in the Standard Model can violate

L symmetry but conserve the current $B - L$, where B is the baryon number. To summarize, since the Majorana terms violate both $B - L$ and L symmetries, these terms can not be used to introduced mass in the Standard Model using perturbation theory or non-perturbative effects [15].

Since these two mechanisms are not useful to explain the origin of the neutrino mass inside the Standard Model, a minimal extension to the SE is proposed in order to provide the neutrinos with mass. This extension consists in inserting right handed neutrinos to the model to explain the origin of the neutrino mass. This extension and its consequences is described in the next section.

3.4 The See Saw Mechanism

The See-Saw mechanism assumes the existance of a neutrino with right helicity. With the existence of this neutrino with right helicity and combining the Dirac and Majorana neutrinos mass terms discussed in the previous sections, the resulting mass Lagrangian would be the shown shown in Equation 3.8, where m_D is a Dirac mass, m_L and m_R are Majorana masses, and h.c is the hermitian conjugate.

$$\mathcal{L}_{mass} = -m_D \left(\overline{\nu}_L \nu_R + \overline{\nu}_R \nu_L\right) - \frac{1}{2}\left(m_L \overline{\nu^C}_L \nu_L + m_R \overline{\nu^C}_R \nu_R\right) + h.c \quad (3.8)$$

If the vector ν is defined as

$$\nu \equiv \begin{pmatrix} \nu_L \\ \nu_R^C \end{pmatrix}$$

then the Lagrangian in Equation 3.8, can be written as in Equation 3.9, where $\mathcal{M}$ is defined in Equation 3.10.

$$\mathcal{L}_{mass} = -\frac{1}{2}\overline{\nu^C}\mathcal{M}\nu + h.c \quad (3.9)$$

$$\mathcal{M} = \begin{pmatrix} m_L & m_D \\ m_D & m_R \end{pmatrix} \quad (3.10)$$

Chapter 4

Computational Resources

The project requires computational work, because simulations of events from the different processes are needed. Also, an analysis of the samples using the analysis code is required. The background and signal samples will be simulated using the software MadGraph [10], Pythia [11] and Delphes [12]. The data analysis and all the subsequent kinematic, topological, and optimal cuts analyses will be performed using ROOT software [13].

MadGraph is an event generator software that allows the simulation of collision between two particle beams. For this analysis in particular, the simulations will consist in proton collision at 13 TeV in order to reproduce the actual conditions of the LHC. MadGraph includes the physical parameters that determine the production probability of a given process, as well as the possible decays of the simulated particles. Besides providing the necessary matrices to calculate the cross sections of the processes, MadGraph also creates the pictorial representations of the Feynman Diagrams from the generated processes. To this end, the software uses perturbation theory in the calculations of production and generation of physical processes.

Pythia is a software that allows the simulation of various strong processes models that evolve from a few bodies to final states with high particle multiplicity. Particularly, in this case Pythia will be used for the simulation of quark and gluon fragmentation processes. This fragmentation process occurs when, due to and intrinsic characteristic of

the strong interaction, there is an energy gain caused by the increase of the distance of two bound quarks. If the separation is enough to reach a critical energy, a pair quark-antiquark is created. The Pythia simulation is necessary, because processes like the ones mentioned above occur during a proton collision at the LHC.

Delphes is a software used to add the effects that a multipurpose detector, like ATLAS or CMS, may have on the particles to the Monte Carlo simulations performed for different processes. In this particular case, Delphes is necessary to simulate the interaction of the particles coming from the generated processes in MadGraph and Pythia with the CMS components. Namely, reproducing the conditions of the detector and the uncertainties coming from the measuring process is achieved by using Delphes. The changes in the cinematic variables due to their interaction with matter, errors caused by the electronics of the detector, and the additional particles generated because of the interaction between the particles and the detector components can be accounted for using Delphes. Other functionalities included in Delphes are: simulation of the detector geometry, the effect of the magnetic field over the particles, and the particle identification and reconstruction efficiencies, among others.

ROOT is a software library developed by CERN to perform data analyses related with particle physics. One of the main characteristics of this library is the possibility of handling large volumes of data efficiently. The latter is achieved by using a tree structure in which the information related with the particles is stored and can be accessed easily using ROOT functionalities. Other features included in the library are the creation of histograms from data trees, multivariate analysis, four-vector calculations, among others. By using ROOT functionalities, it is also possible to estimate optimal cuts in variables to reduce experimental noise to its minimum. This is why the entire final analysis will involve using tools provided by ROOT.

Chapter 5

Signal Simulation

The MadGraph signal simulation was performed assuming that the mass of the heavy neutrino was 1.5 TeV. Also, taking into account that the analysis was going to be performed using Vector Boson Fusion, the paramater of minimum pseudorapidity separation ($\Delta\eta$) between two jets was set to 3.5.

The commands used to generate the desired signal were the following:

- import model SM_HeavyN_NLO
- generate p p > n3 ta+ jj, QCD= 0, n3 > ta+ jj
- add process p p > n3 ta+ jj, QCD= 0, n3 > ta- jj
- add process p p > n3 ta- jj, QCD= 0, n3 > ta- jj
- add process p p > n3 ta- jj, QCD= 0, n3 > ta+ jj

The first command imports the theoretical model that includes the interactions related with the heavy neutrino formation and decay. The next command specifies the processes that are going to be simulated. pp > n3 ta+ jj stands por the proton-proton collision that decays into a heavy neutrino, a τ with positive charge, and two jets. The flag QCD=0 is used to exclude all strong interactions that can be involved in the process. Finally, n3 > ta+ jj is used to force the decay of the

heavy neutrino into a τ charged positively and two jets. The subsequent commands are used to take into account all the possible combinations of the electrical charge that the τ may have.

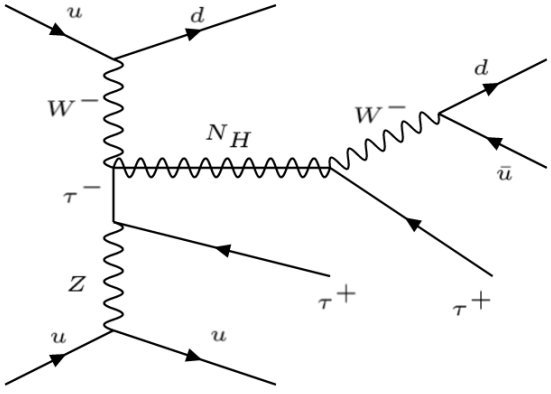

Figure 5.1: Feynman diagram of simulated process involving Z boson

Figures 5.1 and 5.2 show two of the main possible diagrams generated by MadGraph for the processes simulated. These diagrams show the vector boson fusion process, ocurring in Figures 5.1 and 5.2 in the fusion of the W boson with the Z boson and the photon (γ) respectively. In these last two diagrams, the decay of the of the W boson coincides with the one shown in Figure 1.1 for the decay of the W boson resulting in a heavy neutrino and a lepton, which in this case is a τ. The final states for the processes shown in these two diagrams would include two jets coming from the VBF process, two τ's, and two jets coming from the quarks resulting of the W^- decay

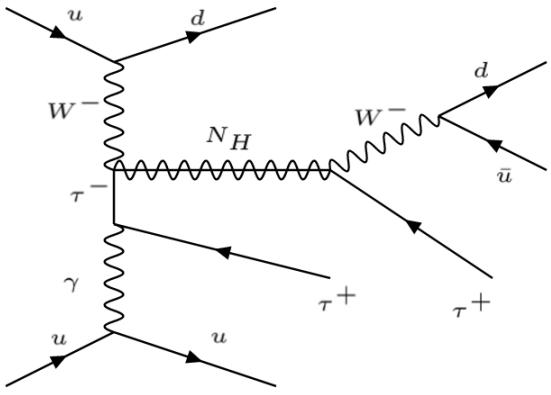

Figure 5.2: Feynman diagram of simulated process involving photon

The simulation was performed in 10 different simulation batches each one containing 10,000 events. Every batch was generated with a different random seed to guarantee the independence of the events between each one of the generated batches. This independance was necessary because the 10,000 event files were merged to form a single file with 100,000 events. As explained earlier, after the events were simulated in MadGraph they were passed to Pythia and then to Delphes so the signal resembled one that could be found at CMS.

Chapter 6

Definitions

6.1 Variable Definitions

The transverse momentum or p_T, is defined as the momentum component that a particle has in the plane perpendicular to the beam line. In the coordinate system of the LHC, this plane corresponds to the $x - y$ plane.

The variable related with the polar angle in the LHC is called pseudorapidity, or η, defined as in Equation 6.1. The use of this variable is justified for mainly two reasons. The first one is that $\Delta\eta$, contrary to $\Delta\theta$, is a Lorentz invariant. This makes $\Delta\eta$ a more natural variable than $\Delta\theta$ for relativistic calculations. The second reason is that the distribution of the values of η in the barrel region, where the multiplicity of particle is less than in the end-caps, is wider allowing the η particle distribution to be aproximately constant.

$$\eta = -\ln\left[\tan\left(\frac{\theta}{2}\right)\right] \tag{6.1}$$

In each event, a maximum of six jets that had a p_T greater than 15 GeV and its absolute value of η less than 5.0 were stored to be analyzed later. Among this list of jets, the two jets whose summed masses resulted in the greatest mass combination were stored and defined as the Di-Jet Pair. The jet with greater momentum in the Di-Jet Pair is the leading jet and the other one in the pair is the sub-leading jet. These two jets

are the ones related with the VBF process. Another variable defined regarding the Di-Jet Pair was the Di-Jet mass and corresponds to the sum of the masses from the jets in the Di-Jet Pair.

With the idea of exploiting the possible difference between signal and background in the p_T for jets and τ's, two new variables shown in Equations 6.2 and 6.3 were defined to check for possible further separation between signal and background. As shown in equation 6.2, the H_T variable is defined as the scalar sum of the jets with p_T greater than 30 GeV and $|\eta| < 5$ that are not B-jets. S_T is defined as the scalar sum of jets that fullfilll the same conditions of H_T, added to the p_T of the τ's in the event.

Since the τ selection is important for this analysis, it is relevant to provide a further description of the preselection criteria for the τ's in the simulated events. For starters, a jet identified as a tau is considered a valid τ if it has a transverse momentum greater than 20 GeV. Also, it was required that a valid τ should not overlap with an electron or a muon. That is, the ΔR, defined as $\Delta R = \sqrt{(\Delta\eta)^2 + (\Delta\phi)^2}$, should not be less than 0.3. This condition guarantees that the jet identified as a τ does not overlap with other leptons. Since the final state for this analysis includes two τ's, the two taus with greater p_T are selected among a maximum of three taus stored for each event. The leading τ is the one with highest p_T and the sub-leading τ is the one with second highest p_T.

$$H_T = \sum_{i=1}^{n} p_T(jet_i) \tag{6.2}$$

$$S_T = \sum_{i=1}^{n} p_T(jet_i) + \sum_{j=1}^{m} p_T(\tau_j) \tag{6.3}$$

6.2 Cut Definitions

In order to achieve a separation between background and signal, several successive requirements for the variables of the particles in the event were made. These requirements are defined as cuts, and for each cut the events that do not comply with the established condition are not

taken into account to fill the histograms. Eight cuts were made to the histograms, storing in each cut the resulting distributions to analyze them later. The first four cuts were related with jets and τ's in the event, and the subsequent four were related with the VBF topology. In the next paragraphs of this section a description of each one of the cuts is given as well as the order in which they were performed.

The first cuts that were made to the histograms were to require that the leading and sub-leading τ's should have a minimum transverse momentum of 20 GeV and a maximum of 2.1 for the absolute value of η. The latter guarantees that the τ's left are detected by the barrel and not the end-caps of the detector. That is an important condition because the detection components, such as the tracker, are in the barrel section and are more accurate than the ones in the end-caps. As a result, a signal detected in the barrel is most certain to be accurate than one detected in an end-cap.

The next cut requires that the event does not have any B-jet. This cut is justified by the fact that one of the main backgrounds for the signal is the top anti-top ($t\bar{t}$) process. The interaction bewteen the top and anti-top quark is related with the production of jets associated with the b quark or B-jets. That is why, much of the $t\bar{t}$ should be eliminated by requiring no B-jets in the event. This fact will be later analized further in chapter 7. The cut that follows the one regarding the B-jets selects the events that have a minimum of two jets with transverse momentum greater than 30 GeV. This two jets must be different from the ones used in the Di-Jet Pair and are the ones that should result from the fragmentation of the quarks resulting of the W decay shown in Figure 1.1.

The last three cuts made to the histograms are related to the VBF topology. The first of the three selects events in which the product of η from the leading and sub-leading jets is negative. This condition guarantees that the jets in the Di-Jet Pair are in opposite hemispheres. The next cut requires that the leading and sub-leading jets of the event have a $\Delta\eta$ greater than 3.8. Finally, the last cut requires that the Di-Jet mass of the event is greater than 500 GeV.

Chapter 7

Distribution Analysis

7.1 Normalized Distributions

The normalized plots are useful to check the shape of backgrounds and signal distributions. These shapes help to identify which variables are not useful for the analysis because the backgrounds overlap with the signal and which variables have to be studied with greater detail because the signal separates from the backgrounds from certain points. An example for both cases is provided in Figures 7.1 and 7.2. In figure 7.1 it can be seen that the signal overlaps for all values with the background distributions. That is why this plot can be used to conclude that the η variable from the sub-leading τ is not useful to isolate the signal from the background. In contrast, the plot in Figure 7.2 show that from around 150 GeV the signal separates from the background distributions. This separation for the p_T of the leading τ suggests that this variable should be examined more closely through the subsequent cuts.

To understand the definition of H_T and S_T mentioned in chapter 6, the plots in Figure 7.3 are shown. The four plots show a separation, in some cases a smaller than others, between the signal and backgrounds distributions. A tendency of the signal jets to have greater transverse momentum than the ones in the backgrounds is shown. This tendency is also displayed for both τ's. Hence, the distributions of H_T and S_T should show a similar behaviour because this variables are the result of

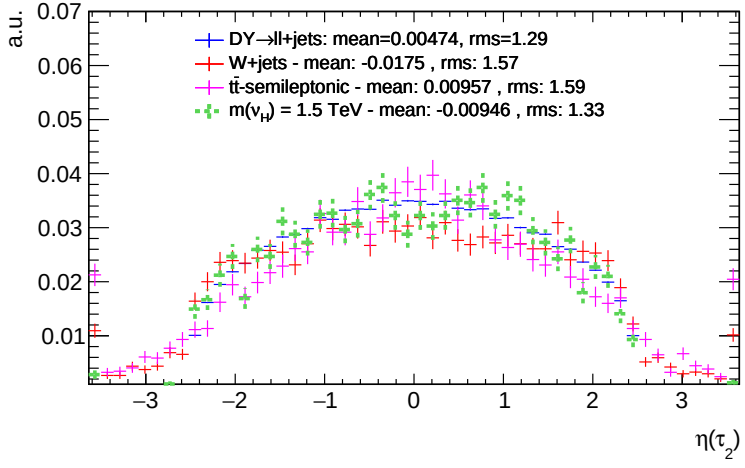

Figure 7.1: Unit plot of η from the sub-leading τ with no cuts

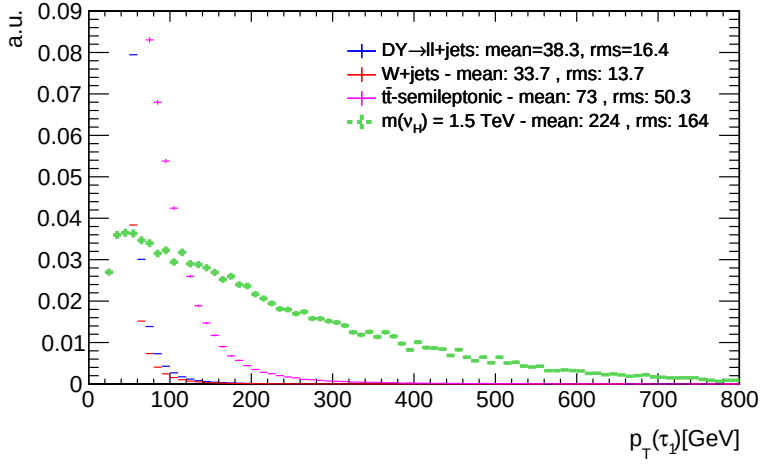

Figure 7.2: Unit plot of p_T of leading τ with no cuts

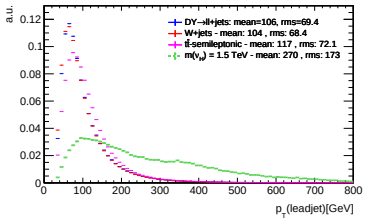

(a) Leading jet p_T unit plot

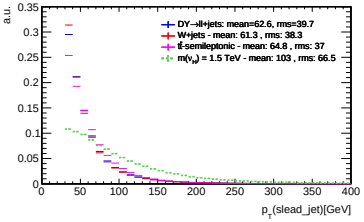

(b) Sub-leading jet p_T unit plot

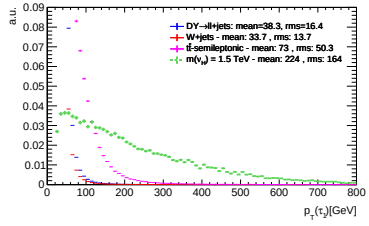

(c) Leading τ p_T unit plot

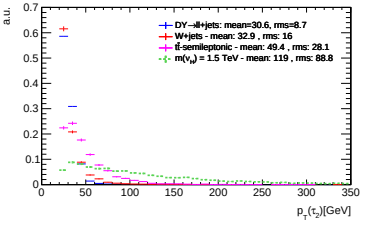

(d) Sub-leading τ p_T unit plot

Figure 7.3: p_T unit plots for different bodies in the event

adding the transverse momentum of jets and τ's in the event.

In Figures 7.4 and 7.5, the normalized plots with no cuts of H_T and S_T are shown. It can be seen that indeed a greater separation between signal and background was achieved. Unlike the distributions of the τ's and jets transverse momentum, the maxima of H_T and S_T lie outside the backgrounds distributions. Furthermore, the background that overlaps at a greater energy with the signal corresponds to $t\bar{t}$. Taking into account what was mentioned in section 6.2, the overlap between the signal and this background could be reduced with the cut related with the number of B-jets in the event. This is why this two variables need to be studied closer in the analysis.

In Figures 7.6 and 7.7, the plots incuding cuts of H_T and S_T respectively are shown. Both plots include all the cuts mentioned in section 6.2. A rebining of the histograms was necessary, because due to the cuts, the number of backgrounds events decreased significantly. This made the error bars for these histograms larger making the analysis of the

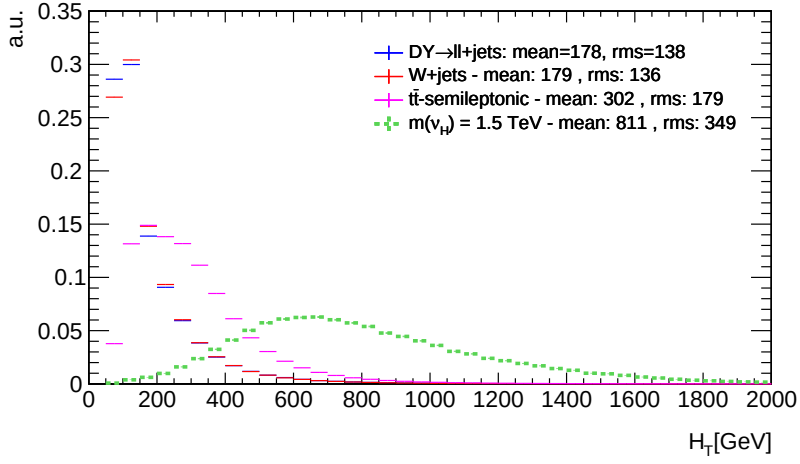

Figure 7.4: Unit plot of H_T with no cuts

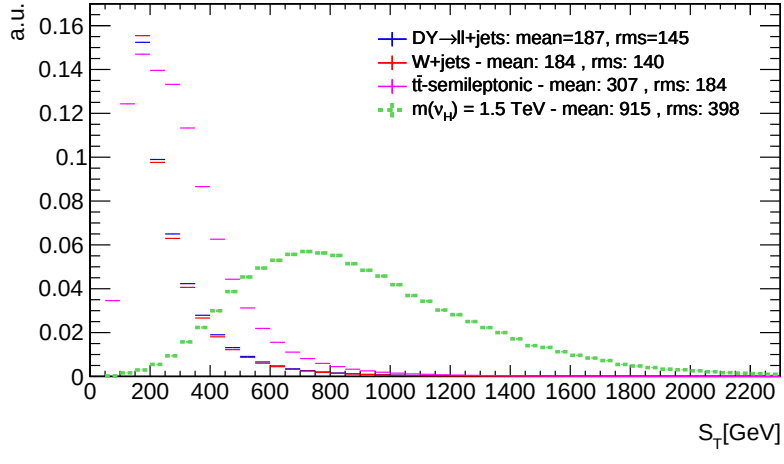

Figure 7.5: Unit plot of S_T with no cuts

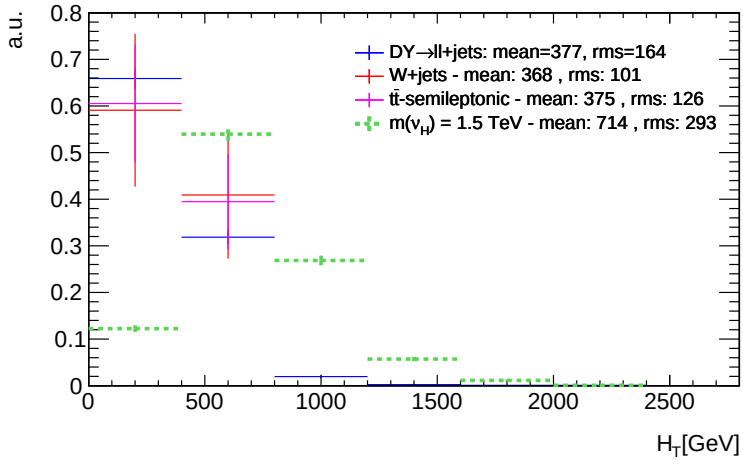

Figure 7.6: Unit plot of H_T with VBF cuts

plot more difficult. For that reason, a bin size of 400 GeV was defined for both of these plots. Comparing the two signal histograms, it can be seen that the maximum of the H_T distribution still overlaps with the background distributions. Although the signal in this case appears on top of the background, it has to be noted that this normalized plots are only useful to get an idea of the distribution shapes. That is why the fact the the signal appears on top of the background does not mean that the signal can be detected over the background for this value. On the contrary, the maximum of the S_T signal distribution has its maximum when the background distributions start to decay. This distribution shape difference between H_T and S_T is related with the fact that the signal has τ's with higher p_T than the ones found in the backgrounds.

The mean values for S_T shown in Figures 7.5 and 7.7 are 915 GeV and 1160 GeV respectively. From the Feynman diagram in Figure 5.2, it can be seen that the jets in the event and one of the taus come from the heavy neutrino decay. Taking into account that the defined mass for the heavy neutrino is 1.5 TeV, it is expected that the maximum of the S_T distribution is around this value. This analysis leads to the

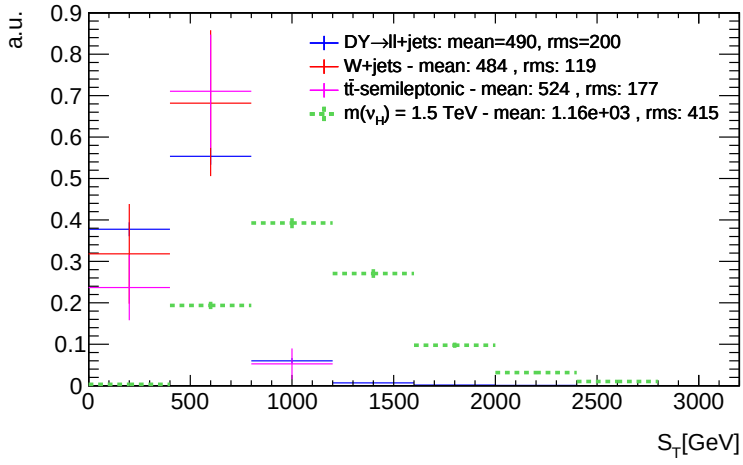

Figure 7.7: Unit plot of S_T with VBF cuts

conclusion that the cuts made to the histograms are helping to select the significant events, because the mean S_T is closer to the expected value after performing all the cuts.

Appendix A

Same Chirality Fields Terms

A field ψ can be decomposed in its chiral components

$$\psi = \psi_R + \psi_L$$

where

$$\psi_R = \frac{1}{2}\left(1 + \gamma^5\right)\psi$$

$$\psi_L = \frac{1}{2}\left(1 - \gamma^5\right)\psi$$

where γ^5 is the fifth Dirac matrix. In a similar way the fields $\bar{\psi_R}$ and $\bar{\psi_L}$ are defined as

$$\bar{\psi_R} = \frac{1}{2}\bar{\psi}\left(1 - \gamma^5\right)$$

$$\bar{\psi_L} = \frac{1}{2}\bar{\psi}\left(1 + \gamma^5\right)$$

Taking into account the previous definitions, the term $\bar{\psi_R}\psi_R$ would be

$$\frac{1}{4}\bar{\psi}\left(1-\gamma^5\right)\left(1+\gamma^5\right)\psi$$

Remebering the property $\left(\gamma^5\right)^2 = 1$, the term $\left(1-\gamma^5\right)\left(1+\gamma^5\right)$ would be zero.

A similar analysis can be performed of the the field with left chirality to obtain the same conclusion. These analysis leads to the conclude that $\bar{\psi_R}\psi_R = \bar{\psi_L}\psi_L = 0$.

Bibliography

[1] Particle Data Group, Olive, K. A. et al. , Chin.Phys. C38, 090001 (2014)

[2] Fukuda, S. et al. (2003) Nuclear Instruments and Methods in Physics Research A 501 (2003) 418–462

[3] Decowski, M. (2016). KamLAND's precision neutrino oscillation measurements. Nuclear Physics B, 908, pp.52-61.

[4] K2K Collaboration: Aliu, E. et al (2005). Evidence for Muon Neutrino Oscillation in an Accelerator-Based Experiment. Physical Review Letters, 94(8).

[5] Nakamura, K. et al. (2010) (Particle Data Group), J. Phys. G 37, 075021 (2010)

[6] Deppisch, F., Bhupal Dev, P., & Pilaftsis, A. (2015). Neutrinos and collider physics. New Journal Of Physics, 17(7), 075019. http://dx.doi.org/10.1088/1367-2630/17/7/075019

[7] Abdesslam, A. et al. (2014) Type II Seesaw Higgsology and LEP/LHC constraints. arXiv:1411.5645 [hep-ph]

[8] Khachatryan, V., Sirunyan, A., Tumasyan, A., Adam, W., Asilar, E., & Bergauer, T. et al. (2016). Search for heavy Majorana neutrinos in $e \pm e \pm +$ jets and $e \pm \mu \pm +$ jets events in proton-proton collisions at s = 8 $\sqrt{s} = 8$ TeV. Journal Of High Energy Physics, 2016(4).

[9] Brooke, J., Buckley, M., Dunne, P., Penning, B., Tamanas, J., & Zgubič, M. (2016). Vector boson fusion searches for dark matter at the LHC. Physical Review D, 93(11). http://dx.doi.org/10.1103/physrevd.93.113013

[10] Alwall, J., Herquet, M., Maltoni, F., Mattelaer, O., & Stelzer, T. (2011). MadGraph 5: going beyond. Journal Of High Energy Physics, 2011(6). http://dx.doi.org/10.1007/jhep06(2011)128

[11] Sjöstrand, T., Ask, S., Christiansen, J., Corke, R., Desai, N., & Ilten, P. et al. (2015). An introduction to PYTHIA 8.2. Computer Physics Communications, 191, 159-177. http://dx.doi.org/10.1016/j.cpc.2015.01.024

[12] de Favereau, J., Delaere, C., Demin, P., Giammanco, A., Lemaître, V., Mertens, A., & Selvaggi, M. (2014). DELPHES 3: a modular framework for fast simulation of a generic collider experiment. Journal Of High Energy Physics, 2014(2). http://dx.doi.org/10.1007/jhep02(2014)057

[13] Antcheva, I., Ballintijn, M., Bellenot, B., Biskup, M., Brun, R., & Buncic, N. et al. (2009). ROOT — A C++ framework for petabyte data storage, statistical analysis and visualization.

[14] Kim, C., & Pevsner, A. (1993). Neutrinos in Physics and Astrophysics (1st ed.). Langhorne, PA: Harwood Academic.

[15] Mohapatra, R., & Pal, P. (1991). Massive neutrinos in physics and astrophysics (1st ed., pp. 31-32). Singapore: World Scientific.